Proceedings of the Seventh International Conference on
Railway Technology: Research, Development and Maintenance
Edited by: J. Pombo
Civil-Comp Conferences, Volume 15, Paper 5.5
Civil-Comp Press, Edinburgh, United Kingdom, 2026
ISSN: 2753-3239, doi: 10.4203/ccc.15.5.5

An Optimized Wind-Tunnel Methodology for Realistic Aerodynamic Investigations of Freight-Trains

J. R. Bell, A. Buhr and L. Siegel

Institute of Aerodynamics and Flow Technology, German Aerospace Center e.V., Göttingen, Germany

Abstract

A wind-tunnel methodology has been developed to improve the accuracy when predicting aerodynamic forces – important for operational efficiency and safety – through more representative modelling of real-world conditions. Measurements taken rail-side in field experiments of the surface-pressure, derived global forces and moments, and the boundary layers around operational freight-trains were used to optimize and subsequently validate the wind-tunnel methodology. The resulting methodology employs boundary layer augmentation – additional surface roughness using spires and Lego blocks – as well as detailed under-body and wagon geometries to achieve similar coefficients of drag, average and fluctuating surface pressure magnitude and surface boundary layers as observed in the real-world.

Keywords: aerodynamics, freight, drag, energy efficiency, crosswinds, boundary layer

1 Introduction

Aerodynamic resistance, drag, is a primary component of the overall resistance to motion a freight train experiences and therefore very important for energy efficiency. This directly affects either emissions or range, depending on the type of power supply; both of which are important considerations for current and future freight operation [1]. Aerodynamics becomes more important with train speed, therefore potential plans of operating from 110 to 160 km/h and faster will only increase this importance.

The presented work is a subset of an overall research project that aims to improve freight-train operational efficiency and safety, through realizable aerodynamic optimization of: freight-train and wagon geometry, loading configuration schemes and infrastructure-vehicle and vehicle-vehicle interaction. The first step of which, presented here, is to have a reliable, accurate wind-tunnel testing methodology, capable of representing real-world operation (illustrated in Figure 1a). To characterize the real-world aerodynamics and provide validation data, measurements have been performed on a full-scale shipping container, the DLR FR8-LAB, that has been transported on normal operating freight-trains in Europe (Figure 1b).

Real-world measurements [2–4] have identified that in the absence of obvious crosswind, infrastructure, or other vehicles, the drag coefficient (C_D) of a container loaded on an operational freight-train is highly dependant on the local loading configuration (distance to container in front, and to the rear of the test-container) and falls within the range of $C_D = 0.10 : 0.50$ [2–4]. The presence of crosswind and infrastructure has been identified to lead to increases of $C_D > 0.70$ [2–4]. Recent investigations using best-practice wind-tunnel methodologies and numerical simulations [5–8], most suitable to be utilized to perform aerodynamic optimizations, due to their controlled environments, have however repeatedly over-predicted drag by up to 50% (with no crosswind or infrastructure interaction modelled), with a range of $C_D = 0.05 : 0.80$ for similar loading configurations compared to full-scale field experiments in the real-world [2–4]. This over prediction of drag in wind-tunnel experiments and simulations is understandable, due to the relative 'cleanness' of the idealized conditions. The work presented aims to add modelling of some of the hypothesised complexity that exists in real-world that until now, hasn't been included in typical wind-tunnel and numerical simulations of freight trains. Namely, geometric 'roughness' on the train's surface and more realistic under-body geometry, to better represent the turbulent, chaotic oncoming flow that a typical container within a freight-train consist experiences, and thus more accurately predict the aerodynamic resistance.

Figure 1: Wind-Tunnel experiment model, at 1:15 scale, with a FR8-LAB test-container, representative gap in front and detailed generic wagon geometry (above) DLR FR8-LAB during field measurements on operational freight-trains in Spain, used as validation for the wind-tunnel methodology developed in the presented work (below).

2 Experimental Methodology

2.1 Wind-Tunnel Setup

The experimental investigation was performed in the crosswind simulation facility Göttingen (SWG), a closed-return 'Göttingen-type' wind tunnel. The test section of the SWG is 2.4 m wide, 1.6 m high and 9 m long. The wind tunnel was set-up for a Reynolds number of $5.5x10^5$ in relation to the test container width, corresponding to an inflow velocity of 50m/s. In this measurement setup a 8.4 m long splitter plate was used, which reduces the effective test-section height to 1.15 m.

Figure 1,2 shows the 1:15 scale, 6.24 m long freight-train model, consisting of a

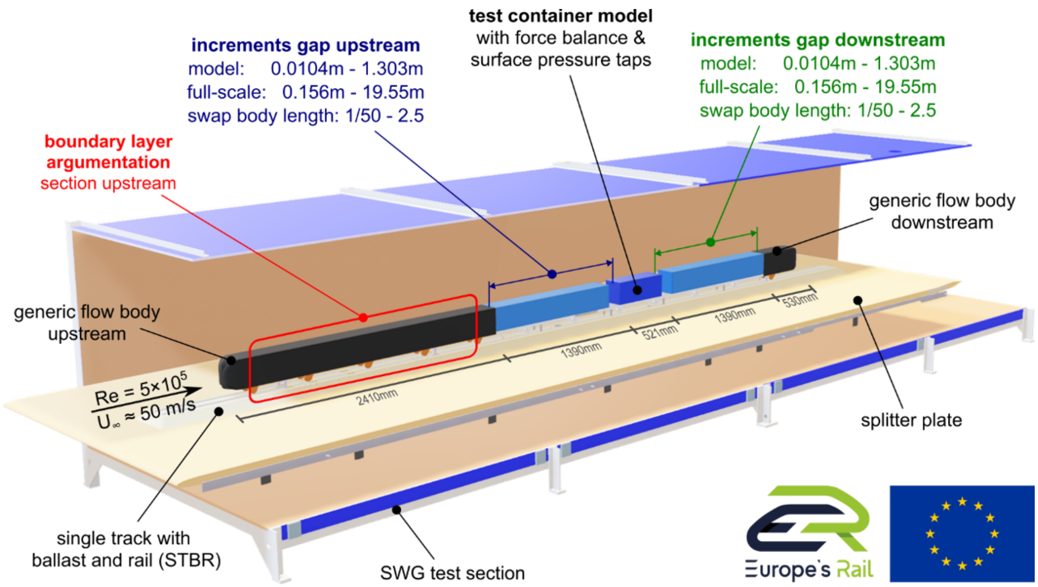

Figure 2: Wind-tunnel experimental setup.

2410 mm upstream and a 530 mm downstream flow body (black) with a scaled freight train cross-section as well as a 3300 mm long modifiable test section (blue) with a test container (dark blue). The wagon geometry, on which the containers were 'loaded', was based on the open-source generic freight-train geometries developed by Corniani et al. [9]. The test-container corresponding to a scaled model of the DLR's FR8-LAB, mounted on a six-component strain-gauge balance onto the freight wagon base to provide a decoupled measurement of the aerodynamic drag force. Furthermore, the test container was equipped with 254 pressure taps to investigate the flow development around the container. In the initial study with incremental change of the gap sizes [5], the modifiable sections were filled with different sized blocks in order to vary the loading gaps up- and downstream. The filler part length corresponded to increments of the test container length, providing full-scale gaps of 0.156m up to 19.55m respectively 0.02 up to 2.5 times the container length.

2.2 Boundary Layer Augmentation

The specifications of the boundary layer augmentations (BLA) devices were informed from wind engineering practices that are applied to replicate atmospheric boundary layers. Irwin-type [10] spires (2D triangular elements) with heights of h=64, 128, 196 & 256mm, widths w= 16, 24 & 32mm and spacing between spires of s=32, 48 & 64 mm were tested. The spire parameters are illustrated in Figure 3a. A fence of height: 48mm was also tested. Roughness was created with single (8x8mm) Lego bricks with flat tiles added on top (total height of 12mm) distributed (48mm spacing) over Lego base plates (Figure 3b). The fences and spires were positioned 240mm and 480mm ($\approx$

$1H\&2H$) respectively from the models nose, with 2m of Lego roughness behind the spires. An example configuration with spires and Lego-roughness applied is presented in Figure 3c. An alternative method of roughness was also tested, by including 5 individual 111mm long gaps (corresponding to 1.65m in full-scale, representative of gaps between containers on different wagons) in the upstream dummy section of the train, with 50% container length (260mm, 3.92m FS) between each gap (visible in Figure 4b).

The boundary layer augmentation devices generate small-scale flow disturbances that, given sufficient convective distances downstream, mix and decay to result in the desired velocity, turbulence intensity and length scale boundary layer profiles at the target area [13-16]. The target area must therefore be located far enough downstream of the spires. An additional complexity in this case is the application of the boundary layer augmentation to a 3D body, not simply a ground plane as in wind engineering applications. Successful application of boundary layer augmentation is therefore generating the intended range of boundary layer profiles without any unintended irregularities in the flow caused by specific elements.

The in-field measurements of real, operational freight-trains determined typical boundary layer displacement thicknesses of approximately 10m (corresponding to 666mm in this 1:15 scaled wind-experiment) with variation across individual trains, and between different trains.

The boundary layer on the model was measured at three longitudinal (x-direction) positions: x1=2455mm, (equivalent to 36.8m in full-scale, FS), x2=3710mm (55.65m FS) and x3=5540mm (83.1m FS). At each longitudinal position, measurements were taken at the centre of the roof, and at lower height of z=93mm (1.4m FS) on the side (corresponding approximately to the TSI/EN14067-4 slipstream measurement height), and again at the side at approximate mid-height of the container (z=183mm, 2.73m FS). The different measurement positions are illustrated in Figure 4, where also different model and BLA configurations are visible.

The boundary layers are characterised by normalised velocity V/V_{inf}, where V_{inf} is the free-stream velocity measured by the reference pitot-static tube positioned above the model in the wind-tunnel.

3 Results

3.1 Boundary Layer

The boundary layer velocity of different BLA methods are presented in Figure 5, highlighting their respective contribution to the roof boundary layer characteristics. The boundary layer on the full 'clean' train body (no BLA) are presented in grey-black points for the three longitudinal positions, showing 'natural' growth along the

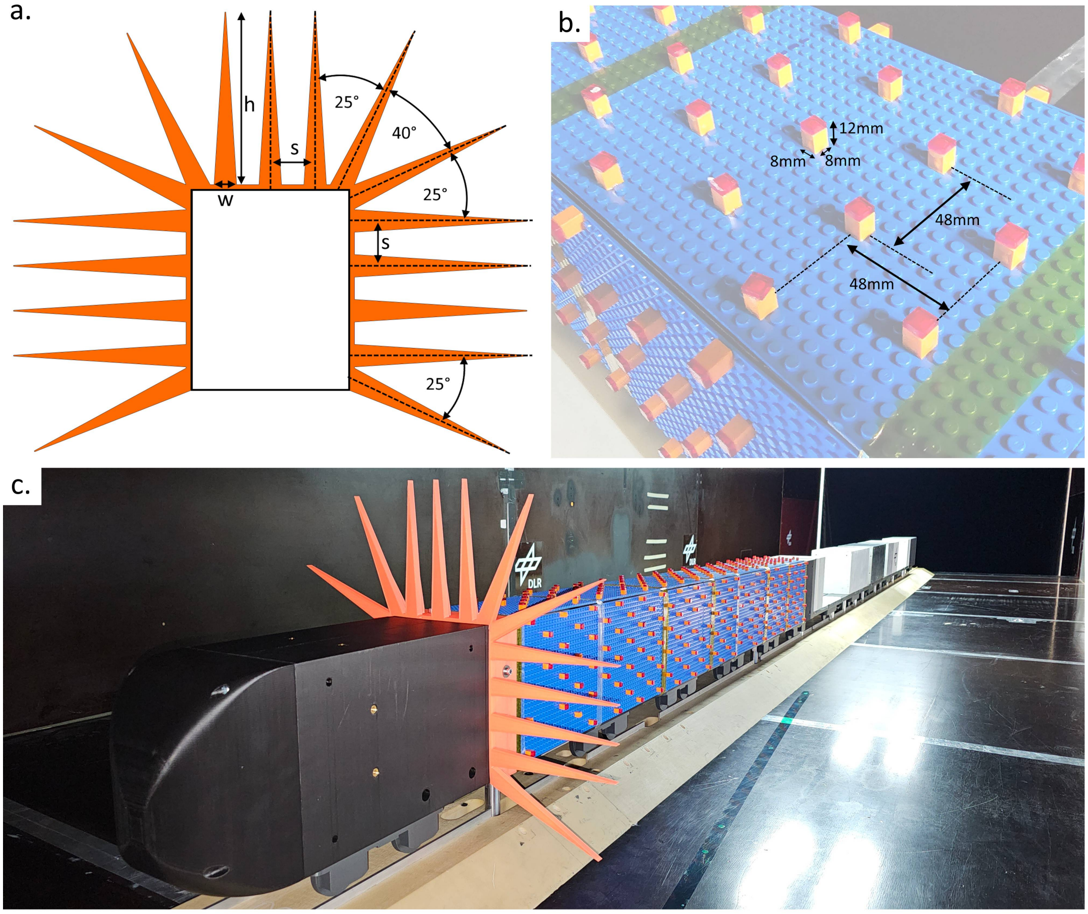

Figure 3: a. Spire dimensions, h: height, s: spacing between spires, w: width of spire. b. Lego-roughness specifications. c. Example of boundary layer augmentation applied to 1:15 model freight-train, with 196mm high spires and lego roughness applied.

Figure 4: Boundary layer measurement positions, a. Side-low, b. Side-mid container height, c. center of roof.

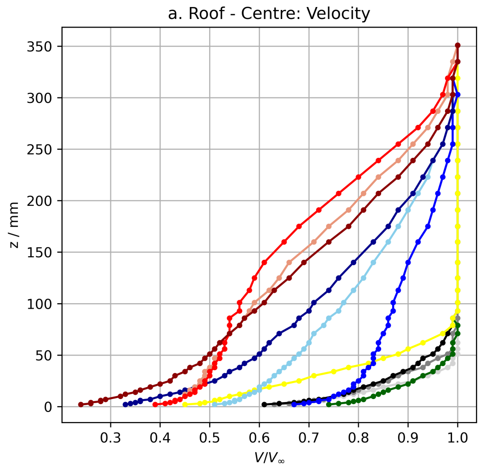

Figure 5: Boundary-layer velocity, measured on the roof centre with different augmentation applied: clean (nothing applied) at x1,2,3, upstream gaps, spires, roughness, fence and their combinations at x1.

5540mm (83.1m FS). All other profiles are presented at position x1 (2455mm, 36.8m FS) for comparison and consistency. The 5 x 110mm gaps in green are shown to have negligible increase relative to the velocity, and only marginal increase in turbulence, equivalent to clean at x3. Alone, simple Lego roughness (yellow points) shows a considerable increase in boundary-layer velocity-deficit - but limited to under 100mm influence from the surface, as one could expect for elements with small dimensions. The 128mm and 256mm tall spires show significant effect, above their respective physical heights, up to 260 and 350mm respectively. However, close to the surface, the velocity-deficit and turbulence profiles are not as curved as the clean profiles. The combination of the spires with Lego-roughness improves the shape of the velocity profiles, appearing as natural developments from the clean profiles. Finally the spires combined with the fence shows interesting results, with an undesirable inflected profile with the 256mm spires, and a reduced velocity-deficit for the 128mm spires - indicating complex interaction between two devices.

The understanding of the contributions and cumulative effects of combining the BLA methods allowed the generation of 6 test boundary layer profiles BLA1-6 whose specifications are listed in Table 1. Their respective velocity and turbulence profiles at each measurement position are presented in Figure 6.

The different augmented boundary layers BLA1-6 show a wide range of velocity and turbulence profile variation. Further, the boundary layer profile at the different measurement positions, roof, side-mid and side-low also exhibit high variation. At the roof (Figure 6a,e), both the velocity and turbulence profiles of BLA6 have a regular form, whilst BLA4 and BLA5 are very similar to each other. In contrast, at both side positions (Figure 6b,c,e,f) BLA6 has a inflected profile, distinctly different to all others, whilst BLA5 has clearly higher velocity deficit and turbulence than BLA4.

BLA#	spire: h,w,s (mm)	lego-roughness	gaps (#, mm)
1	-	-	**5 x 50mm**
2	-	+	-
3	64, 16, 32	+	-
4	128, 16, 32	+	-
5	196, 24, 48	+	-
6	256, 32, 64	+	-

Table 1: BLA1-6 Specifications.

Clearly, the boundary layer around the 3D body of the model train is not constant, and of course, the additional irregular roughness of the under-body wagon geometry and single-track ballast and rail also has an effect.

The full-scale measurements of side-boundary-layers of operational freight trains outlined in [11] measured at mid-container height. Over the range of y=1-9m FS distance from the side-surface (equivalent to 66-600mm here at 1:15 scale) the approximate boundary layer thicknesses were estimated in the range of 5-10m in FS (300-600mm at 1:15 scale). These characteristics found to vary along the train length due to atmospheric wind, even low amounts, as well as due to loading configuration (number and size of gaps). With this real-world data as reference, BLA5 and BLA6 seem to be most representative of realistic boundary layers. With approximate thicknesses at mid-container height of 260 (equivalent to 3.9m in full-scale) and 350mm (5.25m in full-scale) for BLA5 and BLA6 respectively.

Both BLA5 and BLA6 are on the smaller size range measured in full-scale. But this is acceptable, as the real-world measurements were on full-length trains with many gaps in the order of multiple container sizes. In this case, a moderate incoming boundary layer is desired to be modelled before the test-container in the 'arbitrary middle' of a train, that is representative of majority of the train, not the worst case (largest BL possible). Thus, based on this comparison BLA5 and BLA6 are reasonable and were further investigated, along with BLA3 for to assess overall sensitivity.

3.2 Aerodynamic Resistance

The aerodynamic resistance (drag, C_D,) of the test-container in four different loading configurations for the BLA3,BLA5 and BLA6 wind-tunnel are compared to the real-world drag – derived from integrated surface pressure measurements – of the DLR FR8-LAB in Table 2. The loading configurations are characterised by the gap distance

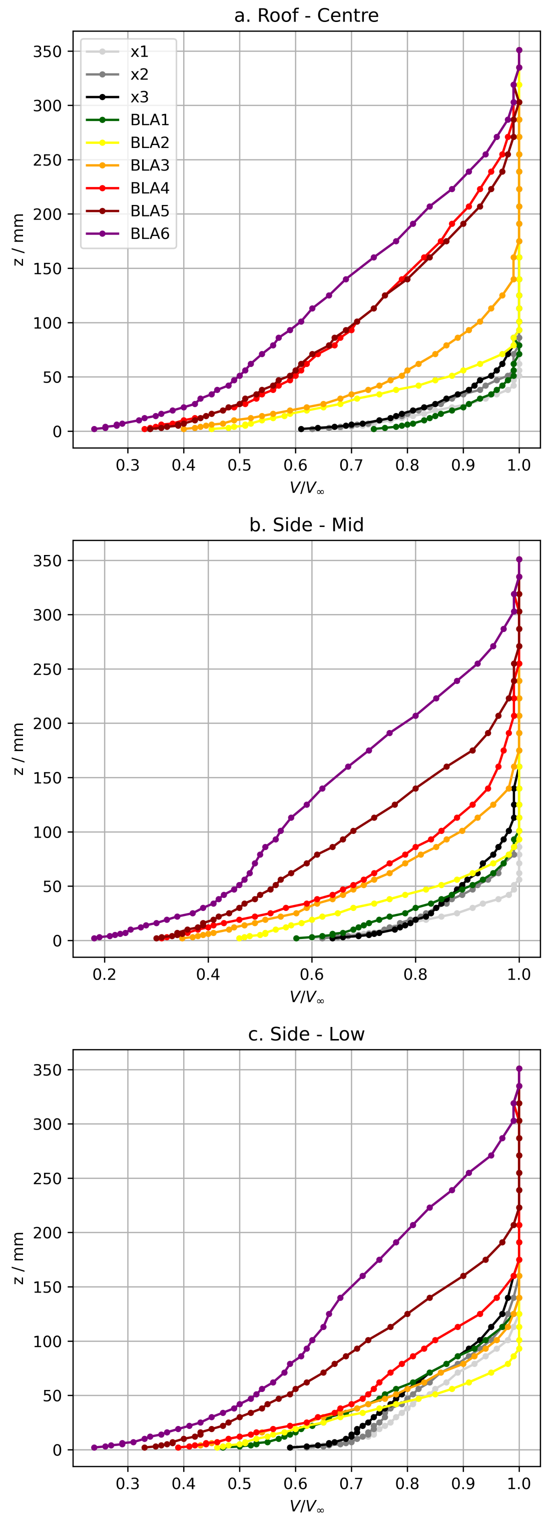

Figure 6: Boundary layer velocity profiles (a,b,c) measured at the roof, side-mid and side-low positions respectively with different augmentation applied. A clean model was measured at longitudinal positions x1,x2,x3, all others presented were measured at x1.

Config.	**FR8-LAB**	**BLA3**	**BLA5**	**BLA6**
$\#1 : f = 1.65m, r = 8.70m$	0.15	0.16	0.14	0.11
$\#2 : f = 8.70m, r = 1.65m$	0.19	0.33	0.26	0.22
$\#3 : f = 14.80m, r = 1.65m$	0.31	0.36	0.29	0.25
$\#4 : f > 20m, r > 20m$	0.39	0.47	0.37	0.32

Table 2: Aerodynamic drag (C_D) of the FR8-LAB container (real-world), compared to the test-container in the wind-tunnel experiment with different boundary layer augmentation applied.

to the container in front (f) and rear (r) of the test-container.

The FR8-LAB results presented below were chosen where no obvious crosswind was present, and no significant interaction with other vehicles or infrastructure was apparent. In such cases, crosswinds or tunnel operation could be expected to significantly vary the drag for a given loading configuration by 25-100% [2–4]. In any case, the FR8-LAB values are still only indicative, as its reasonable to assume they can vary with exact geometry of local containers in front and behind the test-container, specific wagon geometry, minor atmospheric weather conditions, and potentially location within the full train-consist.

Comparison of BLA3, 5 and 6 to the indicative FR8-LAB C_D over the 4 different loading configurations identifies BLA5 as the best case. BLA3, with a significantly smaller and less turbulent boundary layer, over predicts the C_D, for all loading configurations, essentially modelling oncoming flow for the test-container that is too clean and idealised, and thus not representative of the real-world FR8-LAB results. Conversely, BLA6, with its significantly large boundary layer profile and turbulence, generates a dominating boundary layer that reduces the effect of the different loading configurations on the test-containers C_D values. The BLA5 case however, still has a moderate boundary layer – representative of possible real-world conditions – and also shows similar sensitivity of C_D to different loading configurations, with magnitudes comparable to the FR8-LAB within 10-20%

3.3 Surface Pressure

The mean and standard deviation of normalised surface-pressure (C_P) over the test-container in the wind-tunnel is presented in Figure7 with loading configuration $\#3 : f = 14.80m, r = 1.65m$ for BLA3,5,6. In general, high-pressure of $C_P = 0.3 : 0.7$ is visible on the front (windward) surface, with low pressure of $C_P = -0.3 : -0.6$ at the leading edges of the roof and sides surface due to flow separation, and general minimal pressure at the rear ends of the roof, sides and rear vertical surface of $C_P \approx 0$.

At the leading edges on the windward surface, as well as the roof and side corners, high fluctuating pressures are visible with standard deviations in the range of $\sigma_{C_P} = 0.12 : 0.24$, again associated to local flow separation and its inherent transient nature and turbulence.

All three BLA cases show similar pressure distribution and characteristics. However, the magnitude of pressure, and severity of fluctuation decreases from BLA3 to BLA5 and BLA6. This indicates that the larger boundary layer in BLA5 and 6 reduces the local influence of the flow in the gap between the test-container and its interaction with the transient wake of the upstream container. However, as the characteristics are still apparent for all cases, these flow physics exist, but are simply not as dominant and clear. Similarly, even with the significant boundary layers generated with BLA5 and 6, with large velocity deficits and turbulence, the test-containers flow field isn't dominated by the generated boundary layer, the gap flow effect is still apparent.

The mean and standard deviation of normalised surface-pressure (C_P) on the FR8-LAB for the same loading configuration $\#3 : f = 14.80m, r = 1.65m$ is presented in Figure8. The same characteristics and magnitudes of pressure and high fluctuation regions are visible as in the wind-tunnel experiments. In particular, the high-pressure of $C_P \approx -0.5$ on the front, windward surface, and the high fluctuations of $\sigma_{C_P} \approx 0.18$ on the windward edges is relatively similar BLA5, which similarly had the most comparable drag C_D. This further confirms that the flow physics generated in the wind-tunnel experiment, with boundary layer augmentation is representative of real-world operation, providing further confidence in the experimental methodology developed.

4 Conclusions

A wind-tunnel methodology has been developed that applies boundary layer augmentation to a model freight-train - the application of spires, surface roughness as well as a realistic wagon geometry. A variety of different configurations were tested, with the best configuration: BLA5, a combination of spires and roughness identified. This configuration enables the 1:15 test-container model in the wind-tunnel to exhibit a surface boundary-layer, surface-pressure mean and fluctuating distribution, and aerodynamic resistance that is comparable to real-world operational freight-trains. With the wind-tunnel methodology validated against real-world results, the application of the methodology can be applied with greater confidence, in making recommendations for aerodynamic optimization of freight-trains in the future.

Acknowledgements

Funded by the European Union. Views and opinions expressed are however those of the author(s) only and do not necessarily reflect those of the European Union or the Europe's Rail Joint Undertaking. Neither the European Union nor the granting authority can be held responsible for them. The project FP5-TRANS4M-R is supported by the Europe's Rail Joint Undertaking and its members

References

[1] L. Corniani, P. Schito, J. Bell, S. Bruni, ”A review of freight train aerodynamics”, Proceedings of the Institution of Mechanical Engineers, Part F: Journal of Rail and Rapid Transit, 240, 2, 133-150, 2025.

[2] A. Quazi, T. Crouch, J. Bell, T. McGreevy, M.C. Thompson, D. Burton, ”A field study on the aerodynamics of freight trains”, Journal of Wind Engineering and Industrial Aerodynamics, 209, 104463, 2021.

[3] A. Quazi, T. Crouch, J. Bell, T. McGreevy, M.C. Thompson, D. Burton, ”A field study on the aerodynamics of freight trains with different stacking configurations”, Journal of Wind Engineering and Industrial Aerodynamics, 232, 105245, 2023.

[4] J. Bell, A. Buhr, L. Siegel, A. Henning, ”Aerodynamic Optimization of Freight Trains. Part 1: Characterization of real-world operation from a full-scale measurement campaign”, World Congress of Railway Research WCRR, Colorado Springs, USA, 2025.

[5] A. Buhr, L. Siegel, J. Bell, A. Henning, ”Energy savings for freight trains with aerodynamically optimized loading schemes”, ”Proceedings of the Sixth International Conference on Railway Technology: Research, Development and Maintenance”, 7, 3.2, 2024.

[6] A. Buhr, J. Bell, L. Siegel, A. Henning, ”Aerodynamic Optimization of Freight Trains. Part 2: Efficiency and safety recommendations from validated wind-tunnel experiments”, World Congress of Railway Research WCRR, Colorado Springs, USA, 2025.

[7] C. Li, D. Burton, M. Kost, J. Sheridan, M.C. Thompson, ”Flow topology of a container train wagon subjected to varying local loading configurations”, Journal of Wind Engineering and Industrial Aerodynamics, 169, 12-29, 2017.

[8] S. Maleki, D. Burton M.C. Thompson, ”Flow structure between freight train containers with implications for aerodynamic drag”, Journal of Wind Engineering and Industrial Aerodynamics, 188, 194-206, 2019.

[9] L. Corniani, P. Schito, J. Bell, J. Pombo, S. Bruni, ”Aerodynamics of Freight Trains–Addressing the Complexity of Train Geometry through an Open Database”, Promet - Traffic and Transportation, Rethinking the European Railway System, 38, 1, 2026.

[10] H. Irwin, ”The design of spires for wind simulation”, Journal of Wind Engineering and Industrial Aerodynamics, 7, 361–366, 1981.

[11] J. Bell, D. Burton, M.C. Thompson, ”The boundary layer characteristics and unsteady flow topology of full-scale operational inter-modal freight trains”, Journal of Wind Engineering and Industrial Aerodynamics, 201, 104164, 2020

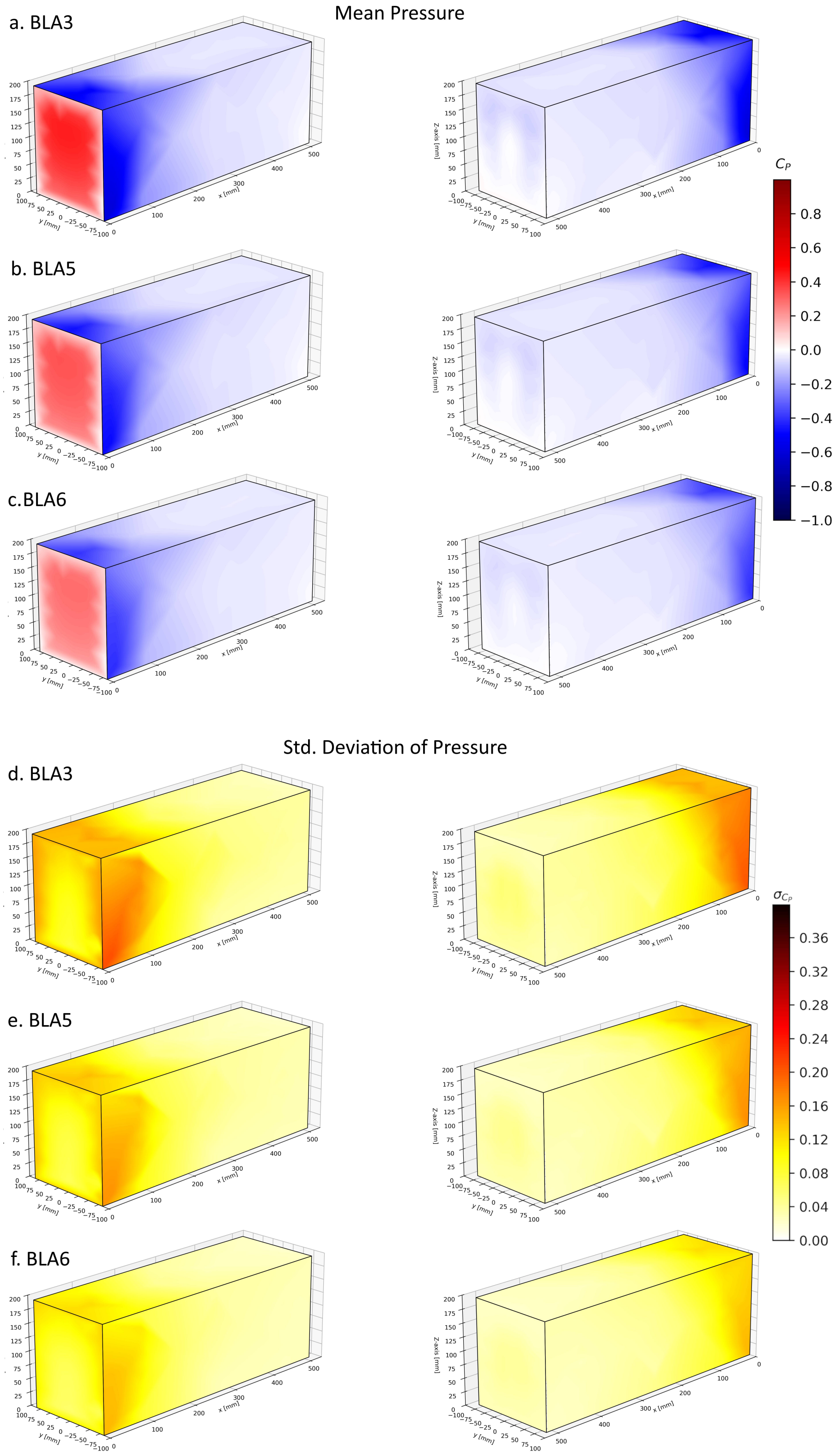

Figure 7: Mean (a,b,c) and standard deviation (d,e,f) of surface-pressure on the front(left) rear (right) of the test-container in the wind-tunnel experiment with a loading configuration $\#3\ :\ f\ =\ 14.80m, r\ =\ 1.65m$ for BLA3, BLA5 and BLA6 cases.

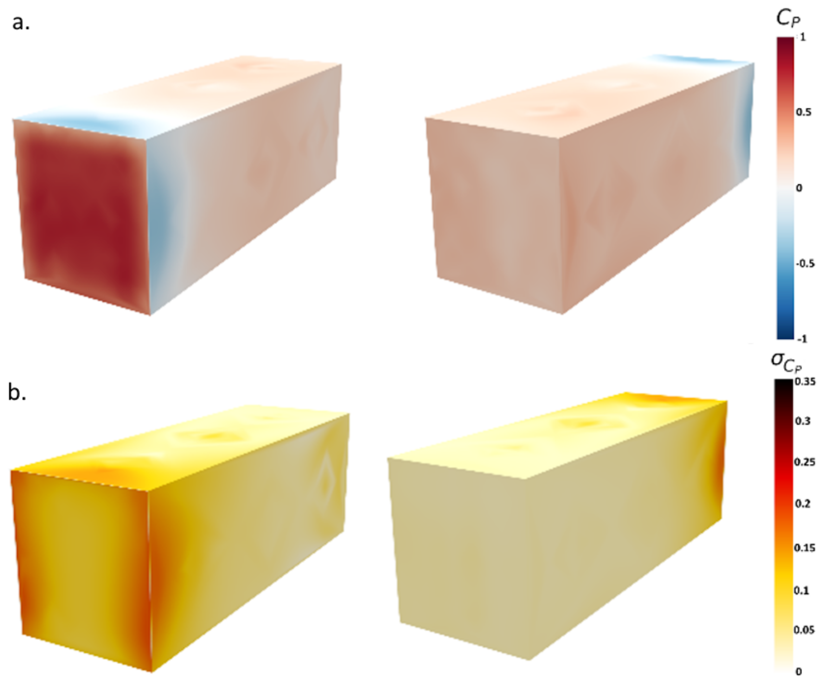

Figure 8: Mean (a) and standard deviation (b) of surface-pressure on the front(left) rear (right) of the FR8-LAB test-container on an operational freight train, with local loading configuration $\#3 : f = 14.80m, r = 1.65m$.